IOPscience iopscience.iop.org

Hyperelastic pressure sensing with a liquid-embedded elastomer

This article has been downloaded from IOPscience. Please scroll down to see the full text article.

2010 J. Micromech. Microeng. 20 125029

(http://iopscience.iop.org/0960-1317/20/12/125029)

View the table of contents for this issue, or go to the journal homepage for more

Download details:
IP Address: 128.237.122.126
The article was downloaded on 06/09/2011 at 21:30

Please note that terms and conditions apply.

IOP PUBLISHING JOURNAL OF MICROMECHANICS AND MICROENGINEERING

J. Micromech. Microeng. **20** (2010) 125029 (6pp) doi:10.1088/0960-1317/20/12/125029

Hyperelastic pressure sensing with a liquid-embedded elastomer

Yong-Lae Park[1,4], Carmel Majidi[2,4], Rebecca Kramer[2], Phillipe Bérard[3] and Robert J Wood[1,2]

[1] Wyss Institute for Biologically Inspired Engineering, Harvard University, Boston, MA, USA
[2] School of Engineering and Applied Sciences (SEAS), Harvard University, Cambridge, MA, USA
[3] Laboratory of Intelligent Systems (LIS), Ecole Polytechnique Fédérale de Lausanne (EPFL), Lausanne 1015, Switzerland

E-mail: rjwood@eecs.harvard.edu

Received 1 September 2010, in final form 25 October 2010
Published 29 November 2010
Online at stacks.iop.org/JMM/20/125029

Abstract
A hyperelastic pressure transducer is fabricated by embedding silicone rubber with microchannels of conductive liquid eutectic gallium–indium. Pressing the surface of the elastomer with pressures in the range of 0–100 kPa will deform the cross-section of underlying channels and change their electric resistance by as much as 50%. Microchannels with dimensions as small as 25 μm are obtained with a maskless, soft lithography process that utilizes direct laser exposure. Change in electrical resistance is measured as a function of the magnitude and area of the surface pressure as well as the cross-sectional geometry, depth and relative lateral position of the embedded channel. These experimentally measured values closely match closed-form theoretical predictions derived from plane strain elasticity and contact mechanics.

1. Introduction

Emerging technologies such as wearable computing [1] and soft active orthotics [2] will depend on stretchable sensors that register deformation and surface pressure. These softer-than-skin sensors must remain functional when stretched to several times their rest length, avoid hysteresis and permanent deformation, and preserve the natural mechanics of the wearer or host system. Hyperelastic transducers for strain and pressure sensing represent just one aspect of the much broader and potentially revolutionary fields of elastically stretchable electronics and computing.

Current approaches to stretchable electronics include buckled (wavy) films of semiconductors for stretchable circuits and diodes [3–5] as well as elastomers that are embedded with microchannels of conductive liquid [6–8]. The latter approach utilizes many of the same molding, embossing and lithography techniques that are used to fabricate soft microfluidic devices [9–11]. One advantage of elastomers is their hyperelasticity, which allows for mechanical durability and stretches as great as 1000%. Such properties are particularly favorable in wearable devices such as adaptive orthotics and insoles that must sustain large deformations and pressures.

Here, we introduce a stretchable, softer-than-skin pressure transducer (figure 1) composed of a silicone rubber (EcoFlex 0030, SmoothOn; PDMS, Dow Corning) sheet embedded with conductive liquid microchannels of non-toxic eutectic gallium–indium (eGaIn, BASF). Pressing the surface of the elastomer deforms the cross-section of nearby channels and changes their electric resistance, as illustrated in figure 2(*a*). The contours in the figure correspond to the vertical displacement of the silicone rubber when surface pressure is applied. Previous efforts in soft pressure sensing and so-called artificial skin include capacitive sensors composed of an elastic insulator layered between conductive fabric [12–14] or a silicone rubber sheet embedded with thin gold film [15]. Other efforts include resistive sensors composed of elastomer embedded with conductive microparticle filler [16–18] or ionic liquid [19–21] and a flexible artificial skin embedded with semiconductor nanowires [22].

This novel design for pressure sensing is adapted from the Whitney strain gauge, which was introduced in 1949 to measure the change in circumferential girth of muscles and limbs [23, 24]. The original Whitney strain gauge

[4] Co-first authors.

 © 2010 IOP Publishing Ltd Printed in the UK & the USA

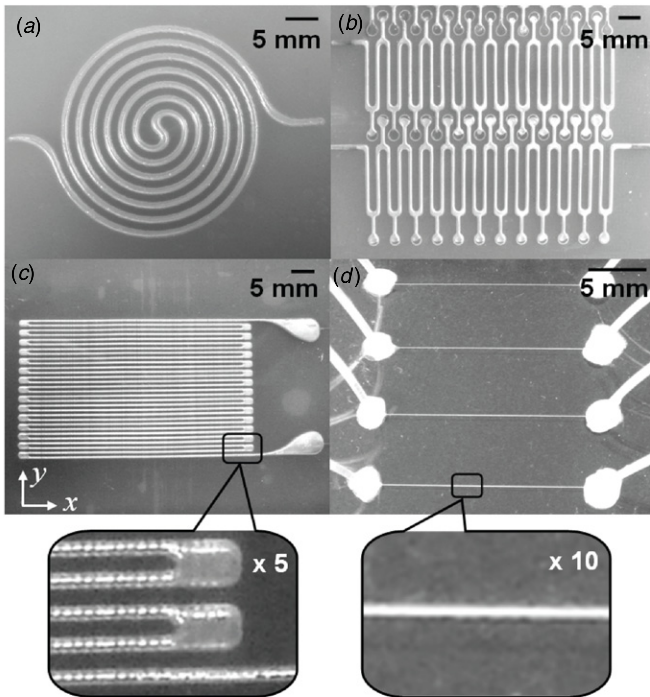

Figure 1. Sheets of polymer are embedded with microchannels of conductive liquid (eGaIn). Surface pressure and in-plane stretching are measured by the electrical resistance change in the conductive channel. (*a*) Spiral-shape channel is for pressure sensing only. (*b*) Serpentine-shape channels with reservoirs are for increased sensitivity. (*c*) Strain gage shape channels are for both pressure and directional strain sensing. ((*a*), (*b*), (*c*)) Silicone rubber (EcoFlex 0030) cast from 3D printed molds with both channel heights and widths of 1 mm, 750 μm and 300 μm, respectively. (*d*) Embedded polydimethylsiloxane (PDMS) microchannels with 20 μm height and (from top) 25, 30, 35 and 40 μm width are produced with a maskless soft lithography process.

was composed of a rubber tube filled with mercury and used a Wheatstone bridge to measure the change in electric resistance of the mercury channel corresponding to stretch. Recently, this principle has been extended to stretchable microelectronics, composed of eGaIn-filled microchannels embedded in polydimethylsiloxane (PDMS) rubber [6]. Embedded channels of eGaIn can operate as a stretchable, mechanically tunable antenna [7] or as strain sensors [8] for measuring stretches of as much as 200%. Here we show that embedded eGaIn channels can also operate as pressure sensors with 1 kPa resolution and 0–100 kPa range. In contrast to strain sensing, the mechanics of pressure sensing are complex and we invoke elasticity and contact mechanics to derive a predictive mathematical model for describing the relationship between external pressure and electrical conductivity. We also produce embedded microchannels with a maskless fabrication method that combines direct laser writing [25, 26] with soft lithography [9, 27] to produce micron-order feature sizes.

2. Fabrication and experimental setup

Sensors with channel dimensions greater than 250 μm are shown in figures 1(*a*)–(*c*). These are produced by casting uncured EcoFlex 0030 silicone rubber (SmoothOn, elastic modulus $E = 125$ kPa) into 3D printed (Connex 500, Objet Geometries Ltd.) molds. After curing under ambient conditions for approximately 4 h, the elastomer layers are removed from the molds and bonded together with a thin, uncured layer of EcoFlex via a process detailed here. To avoid filling the exposed microchannels, the unpatterned elastomer mold is first spin-coated with the thin, uncured layer (1100 rpm for 45 s), which is then partially cured for 30 s at 60 °C in a convection oven. The patterned elastomer mold is then gently bonded to the unpatterned surface. The two elastomer layers (the smooth sheet and the sheet containing the exposed microchannels) are then cured together under ambient conditions for several hours. After the molds are sufficiently bonded together, a syringe is used to fill each channel with eGaIn. Lastly, the ends of the channel are sealed with a final coating of EcoFlex.

Sensors with channel dimensions of 20–300 μm, shown in figure 1(*d*), are fabricated by casting liquid-form PDMS elastomer in an SU-8 mold that is patterned by maskless soft lithography. Photoresist (SU-8 2050) is spun onto a clean silicon wafer at 500 rpm for 10 s (spread), followed by 4000 rpm for 30 s (spin). The wafer is then placed on a hot plate at 65 °C for 3 min and 95 °C for 6 min. Next, the coated wafer is patterned via direct-write laser exposure [25, 26] using a diode-pumped solid-state (DPSS) 355 nm laser micromachining system. The system was previously calibrated to expose a 20 μm thick SU-8 coating to produce channels with 25 to 1000 μm width and $\geqslant$50 μm spacing. The wafer is post-baked on a hot plate at 65 °C for 1 min and 95 °C for 6 min, and consequently developed for 5 min in SU-8 developer. In order to allow for easier removal in subsequent molding steps, a hydrophobic monolayer is introduced through vapor deposition. The patterned wafer is placed in an evacuated chamber (20 mTorr) with an open vessel containing a few drops of trichloro(1H,1H,2H,2H-perfluorooctyl)silane (Aldrich) for 3 h. Next, PDMS (Sylgard 184; Dow Corning, Midland, MI) is cast in liquid form (10:1 mass ratio of elastomer base to curing agent) against the silicon wafer. PDMS is then partially cross-linked in the mold by oven-curing at 60 °C for 30–40 min. Microchannels are constructed by bonding patterned PDMS to unpatterned PDMS via oxygen plasma treatment (Technics Plasma Stripper/Cleaner; 60 W for 30 s). The sealed microchannels are then completely cured at 60 °C overnight. Finally, the microchannels are filled with eGaIn using conventional tubing and syringe dispensing.

The experimental setup for simultaneously measuring applied pressure and electrical resistance is presented in figure 2(*b*). The ends of the eGaIn-filled channels are wired to a precision multimeter (Fluke 8845A). A rigid glass rectangle of width a and length L is pressed into the sensor with a digital height gauge (Swiss Precision Instruments, Inc.). In order to distribute the pressure more uniformly and better simulate tactile or elastic contact, a 5 mm thick sheet of elastomer with the same area as that of the glass rectangle is inserted between the glass and the sensor surfaces. The sensor is supported by an electronic scale (6000 g OHAUS Scout Pro) that measures the total force F exerted on the surface. The average

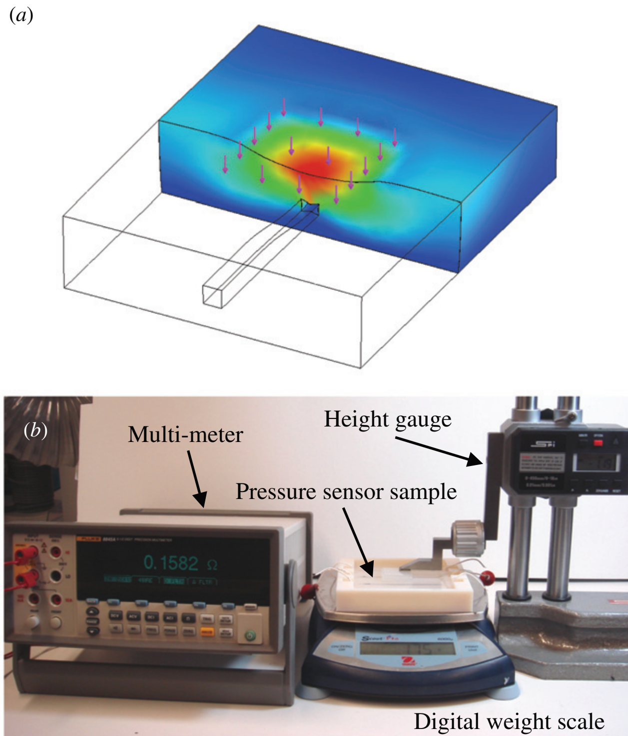

Figure 2. (*a*) Pressing the surface of the elastomer reduces the cross-sectional area of the embedded liquid channel and increases its electrical resistance. Contours represent the vertical displacement of the silicone rubber. (*b*) Experimental setup for simultaneously measuring applied pressure and electrical resistance for a sheet of silicone rubber embedded with a straight channel of conductive liquid.

(This figure is in colour only in the electronic version)

pressure exerted over the area of contact is calculated as $p = F/aL$.

3. Results

The change in electrical resistance ΔR of the embedded, conductive liquid-filled channels is measured as a function of the applied pressure p using the experimental setup presented in figure 2(*b*). Both experimentally measured values (open circles) and theoretical predictions (solid curve) are plotted in figure 3 for an elastomer containing a straight channel with width $w = 2$ mm, height $h = 1$ mm, and with a top face that is at a distance $z = 2$ mm from the surface of the elastomer. Pressure is applied over an area of length $L = 27$ mm and width $a = 25$ mm. For this set of measurements, the major axis of the contact area (which has length L) is aligned with the centerline of the channel. The plot contains data points from multiple loading and unloading cycles, demonstrating significant repeatability and low hysteresis.

As shown in the plot, the change in electrical resistance ΔR increases exponentially with applied pressure. This curve closely matches the theoretical prediction, which is represented by the solid line. It is important to note that no data fitting is used; the theoretical curve is derived entirely from the prescribed geometry, the prescribed pressure, the

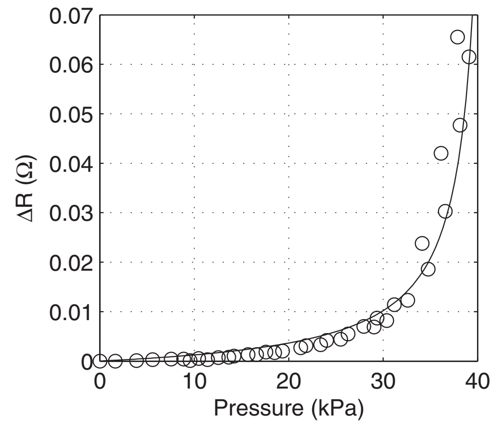

Figure 3. Experimental (open circles) and theoretical results (solid line) for the change in electrical resistance ΔR as a function of applied pressure for a contact area of width $a = 25$ mm and length $L = 27$ mm. The channel has a width $w = 2$ mm, height $h = 1$ mm, and top face that is at a distance $z = 2$ mm from the surface. The theoretical prediction (1) is based on an electrical resistivity of $\rho = 29.4 \times 10^{-8}\ \Omega\ \mathrm{m}^{-1}$ and an independently measured elastic modulus of $E = 125$ kPa.

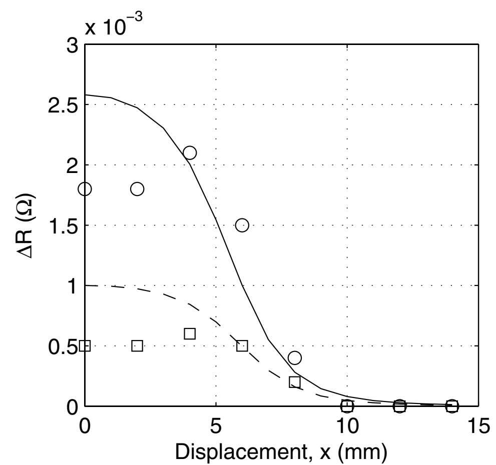

Figure 4. Change in electrical resistance ΔR as a function of lateral displacement (x). The open squares and circles correspond to experimental measurements for applied pressure p of 25 and 15 kPa, respectively. The solid and dashed lines are the corresponding theoretical predictions (see equations (3) and (4)); $a = 25$ mm, $L = 27$ mm, $z = 3$ mm, $w = 2\ 2$ mm, $h = 1$ mm.

known resistivity $\rho = 29.4 \times 10^{-8}\ \Omega\ \mathrm{m}^{-1}$ of eGaIn [6] and the elastic modulus $E = 125$ kPa of the rubber, which are independently measured by comparing the pressure with the depth of indentation. The closed-form theoretical solution and derivation are presented in the next section.

As expected, ΔR decreases the further the channel is from the center of applied pressure. Figure 4 presents a plot of ΔR versus lateral displacement x for pressures $p = 15$ kPa and $p = 25$ kPa. As illustrated in figure 5, x is defined as the horizontal distance between the channel centerline and the major axis of the contact area. For both pressures, the signal ΔR decreases significantly with increasing relative displacement. The theoretical predictions, which are represented by dashed and solid curves for 15 and

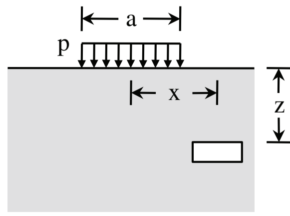

Figure 5. Two-dimensional, plane strain representation of elastomer embedded with a microchannel of width w and height h. The surface of the elastomer is subject to a pressure p uniformly distributed over a width a.

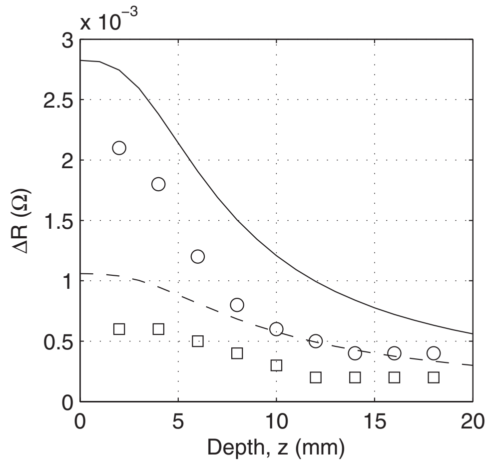

Figure 6. Change in electrical resistance ΔR as a function of channel depth z. The open squares and circles correspond to experimental measurements for applied pressure p of 25 and 15 kPa, respectively. The solid and dashed lines are the corresponding theoretical predictions (see equations (3) and (4)); $a = 25$ mm, $L = 27$ mm, $x = 0$ mm, $w = 2$ mm, $h = 1$ mm.

25 kPa, respectively, are reasonably consistent with experimental measurements, which correspond to the open squares and circles. While the surface pressure is approximately uniform, there are small stress concentrations near the edges of the contact zone. Hence, when $x = 4$ mm and the channel is between the center and the edge of the contact zone, the nominal stress is slightly greater and a larger response ΔR is measured.

Lastly, a plot of ΔR versus channel depth z (for $x = 0$) is presented in figure 6. Referring to figure 5, z is defined as the distance between the surface of the elastomer and the top wall of the channel. As demonstrated in the experimental results, the resistance change ΔR decreases the farther the channel is from the surface. This trend is also predicted by the theory, although the theory appears to overestimate the absolute change by as much as a factor of 2.

4. Theory

The mechanics of the microchannel embedded elastomer are complex and can only be modeled with an approximate mathematical analysis. For the sake of simplicity, consider a two-dimensional representation of a straight channel with rectangular cross-section embedded in an elastomeric halfspace. As illustrated in figure 5, the channel has width w, height h, and a top wall that is at a distance z from the surface of the elastomer.

A uniform external pressure p is applied to the surface of the elastomer over an area of width a. As shown in figure 5, the centers of the channel and the area of applied pressure are offset horizontally by a distance x. For channels close to the center of the applied pressure (i.e. $|x| < a/2$ and $z < a$), elastic deformation will reduce the cross-sectional area and hence increase electric resistance. The reduction in cross-sectional area is primarily governed by the magnitude of the vertical component of the stress tensor: $\sigma_z = \sigma_z(x, z; p, a)$. Since the applied pressure is compressive, σ_z will have a negative sign.

As in the case of crack growth in linear elastic fracture mechanics (LEFM), the field lines of the internal stress σ_z will concentrate about the edges of the microchannel [28, 29]. This is in order to satisfy the boundary condition of zero traction on the walls of the channel. Because the channel is filled with fluid, the walls will not be traction free but are instead subject to hydrostatic pressure. However, this internal channel pressure is considered negligible in comparison to the induced nominal stress σ_z and so zero traction is assumed.

According to LEFM, an average vertical stress σ_z applied in the vicinity of a crack will increase the gap between the crack faces by an amount $\Delta h = 2(1 - \nu^2)w\sigma_z/E$, where ν is Poisson ratio and E is the elastic modulus [28]. Because the microchannels are small compared to the dimensions of the elastomer, their influence on the stress distribution will be negligible except in the immediate vicinity of each channel. Therefore, for channels below the area of contact ($|x| < a/2$ and $z < a$), the average stress in the neighborhood of the channel may be approximated as $\sigma_z = -p$. Substituting this into the expression for Δh implies that the total change in electrical resistance will be approximately

$$\Delta R = \frac{\rho L}{wh}\left\{\frac{1}{1 - 2(1 - \nu^2)wp/Eh} - 1\right\}. \tag{1}$$

In general, p should be replaced with χp, where $\chi = \chi(x, z)$ is a correction that depends on the relative position (x, z) of the channel centerline. The correction $\chi = -\sigma_z/p$ is obtained by solving σ_z using Boussinesq's method: [30]

$$\sigma_z = \int_{-a/2}^{a/2}\int_{-\infty}^{\infty} -\frac{3pz^3}{2\pi}\{(x - X)^2 + Y^2 + z^2\}\,\mathrm{d}Y\,\mathrm{d}X. \tag{2}$$

A closed-form, elementary expression for σ_z is obtained with *Maple 13* (Waterloo Maple Incorporated, 2009). Solving for χ yields

$$\chi = \frac{c_1 c_2 - c_3}{c_4}, \tag{3}$$

where

$$c_1 = \tan^{-1}\left(\frac{a + 2x}{2z}\right) + \tan^{-1}\left(\frac{a - 2x}{2z}\right)$$
$$c_2 = -8x^2a^2 + 32x^2z^2 + 8z^2a^2 + 16x^4 + 16z^4 + a^4$$
$$c_3 = -16zax^2 + 4za^3 + 16z^3a$$
$$c_4 = \pi(4x^2 + 4xa + a^2 + 4z^2)(4x^2 - 4xa + a^2 + 4z^2).$$

This is used to evaluate the change in electrical resistance as a function of x and z:

$$\Delta R = \frac{\rho L}{wh}\left\{\frac{1}{1 - 2(1 - \nu^2)w\chi p/Eh} - 1\right\}. \tag{4}$$

5. Discussion

As demonstrated in figures 3, 4 and 6, the theory is consistent with the experimental measurements for a wide range of pressures p and relative positions (x, z). In figures 4 and 6 there appears to be close to 50% discrepancy between the theory and the experiment. This is due to the simplifying assumptions of the theoretical model, which is based on plane strain linear elasticity, ignores the influence of the channel on global stress distribution, and assumes uniform channel collapse with zero surface traction and constant width. Relaxing these assumptions will lead to a more accurate theoretical prediction that better matches the experimental result. However, these models require numerical computations or finite element analyses that will not yield an algebraic closed-form solution, such as the one presented in (4).

In addition to capturing the principal mechanics of the elastomer pressure transducer, the theory reveals several key properties that can be exploited for customized functionality. The first property allows for mechanical decoupling between pressure sensing and stretch sensing. This is critical in being able to distinguish whether the change in microchannel conductivity is induced by pressure or stretching. The second property relates to the sensor bandwidth, i.e. the range of pressures that the sensor can detect.

Sensor response to pressure and stretch are decoupled by selecting the appropriate microchannel depth z and path (e.g. straight, serpentine and spiral). As demonstrated in figure 6, the sensor response vanishes as z exceeds the width a of the contact area. In contrast, the change in electrical resistance due to channel elongation is *invariant* with microchannel depth. Instead, elongation response is governed by the simple formula $\Delta R/R_0 = \lambda^2 - 1$, where $R_0 = \rho L/wh$ is the original resistance of the unstretched channel and the stretch $\lambda = L_f/L$ is the ratio of the stretched length L_f to the natural length L. This implies that a microchannel embedded deep within the elastomer (a distance $z > a$ from the surface for anticipated values of a) will only measure stretch and not pressure. Alternatively, a spiral-shaped microchannel embedded close to the elastomer surface, as shown in figure 1(*d*), will detect pressure but not uniaxial stretching. This is because increased electrical resistance in one direction is balanced by reduced resistance in the perpendicular direction.

Sensor bandwidth is controlled by a characteristic pressure $\hat{p} = Eh/w$ and thus depends only on the elastic modulus E of the elastomer and the aspect ratio h/w of the microchannel cross-section. Noting that $R_0 = \rho L/wh$ is the natural resistance of the channel, it follows from (1) that for a channel embedded near the surface of the elastomer, $\Delta R/R_0 = 1/(1 - 2(1 - \nu^2)p/\hat{p})$. Depending on the ratio $p/\hat{p}$, the relative change in electrical resistance can range from fractions of a percent to orders of magnitude. Consider, for example, EcoFlex ($E = 125$ kPa) embedded with a microchannel of width $w = 100$ μm and thickness $h = 20$ μm. In response to a typical keystroke pressure in the range of 1–10 kPa, the electrical resistance of the embedded microchannel would change by an order of 1%. In contrast, peak pressure in foot–ground contact during walking is in the order of 100 kPa, which would result in an approximately 50% change in electrical resistance. For all applications, the design parameters E and h/w should be selected such that the characteristic pressure $\hat{p}$ is comparable to the range of anticipated pressures p.

6. Conclusion

A hyperelastic pressure sensor is introduced that measures pressures in the range of 0–100 kPa with 1 kPa resolution. The sensor is composed of a soft elastomer that is embedded with eGaIn-filled microchannels. The width of the microchannels ranges from 25 μm to 2 mm. They are fabricated by casting the elastomer in molds that are produced with either a 3D printer (250 μm to 2 mm channel dimensions) or laser-based soft lithography (25−300 μm). Applying pressure to the surface of the elastomer deforms the underlying channel and reduces its electrical resistivity. For pressures in the range of 0–100 kPa, the resistance changes by tens of milli-ohms (mΩ), as much as 50% of the original resistance. The relationship between the change in resistance ΔR, pressure p and geometry are captured by an algebraic, closed-form equation that is derived from theories of plane strain elasticity, contact mechanics and LEFM.

Future efforts will focus on integrating the hyperelastic sensors into orthotic devices and soft robots in order to sense pressure and ground contact. The principles and fabrication techniques presented here may also be used to explore other potential sensing modes and electronic functions. Lastly, the theoretical analysis can be applied or modified to predict sensor performance for a broad range of designs, length scales and materials.

Acknowledgments

The authors thank Leia Stirling and Geordie Malcomson at the Wyss Institute, and Xin Chen in the Department of Chemistry (Harvard) for helpful discussions. This work was funded by the Wyss Institute (YLP) and the National Science Foundation, award no DMR-0820484 (CM, RK). Any opinions, findings and conclusions or recommendations expressed in this material are those of the authors and do not necessarily reflect those of the National Science Foundation.

References

[1] Marculescu D *et al* 2003 Electronic textiles: a platform for pervasive computing *Proc. IEEE* **91** 1995–2018

[2] Stirling L, Yu C-H, Miller J, Wood R, Goldfield E and Nagpal R 2010 Applicability of shape memory alloy wire for an active, soft orthotic *Proc. Int. Conf. Shape Memory and Superelastic Technologies (Pacific Grove, CA)* pp 20–1

[3] Rogers J A and Huang Y 2009 A curvy, stretchy future for electronics *Proc. Natl Acad. Sci. USA* **106** 10875–6

[4] Khang D-Y, Jiang H, Huang Y and Rogers J A 2006 A stretchable form of single-crystal silicon for high-performance electronics on rubber substrates *Science* **311** 208–12

[5] Kim D-H, Ahn J-H, Choi W M, Kim H-S, Kim T-H, Song J, Huang Y Y, Liu Z, Lu C and Rogers J A 2008 Stretchable and foldable silicon integrated circuits *Science* **320** 507–11

[6] Dickey M D, Chiechi R C, Larsen R J, Weiss E A, Weitz D A and Whitesides G M 2008 Eutectic gallium–indium (EGaIn): a liquid metal alloy for the formation of stable structures in microchannels at room temperature *Adv. Funct. Mater.* **18** 1097–104

[7] So J-H, Thelen J, Qusba A, Hayes G J, Lazzi G and Dickey M D 2008 Reversibly deformable and mechanically tunable fluidic antennas *Adv. Funct. Mater.* **18** 1097–104

[8] Kim H-J, Son C and Ziaie B 2008 A multiaxial stretchable interconnect using liquid-alloy-filled elastomeric microchannels *Appl. Phys. Lett.* **92** 011904

[9] Duffy D C, McDonald J C, Schueller O J A and Whitesides G M 1998 Rapid prototyping of microfluidic systems in poly(dimethylsiloxane) *Anal. Chem.* **70** 4974–84

[10] Unger M A, Chou H-P, Thorsen T, Scherer A and Quake S R 2000 Monolithic microfabricated valves and pumps by multilayer soft lithography *Science* **288** 113–6

[11] Quake S R and Scherer A 2000 From micro- to nano-fabrication with soft materials *Science* **290** 1536–40

[12] Hoshi T and Shinoda H 2006 Robot skin based on touch-area-sensitive tactile element *Proc. IEEE Int. Conf. on Robotics and Automation (ICRA '06) (Orlando, FL, May 2006)* pp 3463–8

[13] Chigusa H, Makino Y and Shinoda H 2007 Large area sensor skin based on two-dimensional signal transmission technology *Proc. IEEE EuroHaptics Conf. and Symposium on Haptic Interfaces for Virtual Environment and Teleoperator Systems (WHC '07) (Tsukuba, Japan, March 2007)* pp 151–6

[14] Yoshikai T, Fukushima H, Hayashi M and Inaba M 2009 Development of soft stretchable knit sensor for humanoids' whole-body tactile sensibility *Proc. IEEE-RAS Int. Conf. on Humanoid Robots (ICHR '09) (Paris, France, Dec. 2009)* pp 624–31

[15] Cotton D, Graz I M and Lacour S P 2009 A multifunctional capacitive sensor for stretchable electronic skins *IEEE Sensors J.* **9** 2008–9

[16] Alirezaei H, Nagakubo A and Kuniyoshi Y 2007 A highly stretchable tactile distribution sensor for smooth surfaced humanoids *Proc. IEEE-RAS Int. Conf. on Humanoid Robots (ICHR '07) (Pittsburgh, PA, Nov. 2007)* pp 167–73

[17] Ventrelli L, Beccai L, Mattoli V, Menciassi A and Dario P 2009 Development of a stretchable skin-like tactile sensor based on polymeric composites *Proc. IEEE Int. Conf. on Robotics and Biomimetics (ROBIO '09) (Guilin, China, Dec. 2009)* pp 123–8

[18] Lacasse M-A, Duchaine V and Gosselin C 2010 Characterization of the electrical resistance of carbon-black-filled silicone: application to a flexible and stretchable robot skin *Proc. IEEE Int. Conf. on Robotics and Automation (ICRA '10) (Anchorage, AK, May 2010)* pp 4842–8

[19] Wettels N, Santos V J, Johansson R S and Loeb G E 2008 Biomimetic tactile sensor array *Adv. Robot.* **22** 829–49

[20] Tseng W-Y, Fisher J S, Prieto J L, Rinaldi K, Alapati G and Lee A P 2009 A slow-adapting microfluidic-based tactile sensor *J. Micromech. Microeng.* **19** 085002

[21] Noda K, Iwase E, Matsumoto K and Shimoyama I 2010 Stretchable liquid tactile sensor for robot-joints *Proc. IEEE Int. Conf. on Robotics and Automation (ICRA '10) (Anchorage, AK, May 2010)* pp 4212–7

[22] Takei K, Takahashi T, Ho J C, Ko H, Gillies A G, Leu P W, Fearing R S and Javey A 2010 Nanowire active-matrix circuitry for low-voltage macroscale artificial skin *Nature Mater.* **9** 821–6

[23] Whitney R J 1949 The measurement of changes in human limb-volume by means of a mercury-in-rubber strain gauge *Proc. Physiol. Soc.* **109** 5–6

[24] Rastrelli L U, Anderson E L and Michie J D 1967 Elastomeric strain gauge *US Patent* 3,304,528

[25] Pique A, Chrisey D B, Fitz-Gerald J M, McGill R A, Auyeung R C Y, Wu H D, Lakeou S, Nguyen V, Chung R and Duignan M 1967 Direct writing of electronic and sensor materials using a laser transfer technique *J. Mater. Res.* **15** 1872–5

[26] Menon R, Patel A, Gil D and Smith H I 2005 Maskless lithography *Mater. Today* **8** 26–33

[27] Xia Y and Whitesides G M 1998 Soft lithography *Annu. Rev. Mater. Sci.* **28** 153–84

[28] Tada H, Paris P C and Irwin G R 2000 *The Stress Analysis of Cracks Handbook* 3rd edn (New York: ASME Press)

[29] Anderson T L 2005 *Fracture Mechanics: Fundamentals and Applications* 3rd edn (Boca Raton, FL: Taylor and Francis)

[30] Anderson T L 2005 *Theory of Elasticity* 3rd edn (New York: McGraw-Hill)